DESIGN, SIMULATION AND EXPERIMENTAL INVESTIGATION OF 3D PRINTED MECHANICAL METAMATERIALS

Sunil Magadum†*, Amol Gilorkar*, Deepak M*, Rakshith B S*, Navaharsha P*, Nagahanumaiah† and Somashekara M A*

†Central Manufacturing Technology Institute, Bengaluru 560022
*Department of Mechanical Engineering, Indian Institute of Technology, Dharwad 580011

Abstract

Mechanical metamaterials have generated special interest recently due to their tailorable structure, exceptional mechanical properties, and advancements in 3D printing processes that allow the fabrication of intricately structured components. Designing innovative structures of metamaterials will lead to the development of advanced materials with special properties. The experimental investigation presented in this paper involves the design, simulation, fabrication, and testing of three different mechanical metamaterial models i.e. Chiral, Re-entrant, and Hybrid printed in acrylonitrile styrene acrylate (ASA) using fused deposition modeling (FDM). Subsequently, a uniaxial compression test and ex-situ characterization was performed for studying the mechanical properties, the types of fracture and crack propagation of the printed metamaterial models which may lead to the development of metamaterials with tunable compressive/bending stiffness.

Keywords: 3D Printing, Mechanical Metamaterials, Chiral, Re-entrant, Hybrid Model

1. Introduction

A metamaterial is a non-natural architecture design that is produced to get extraordinary properties that are not present in naturally existing materials [1]. Repeated unit patterns of small to large scales are used to get the desired metamaterial design. The properties of the materials such as stiffness, poisson's ratio, force absorption capability, or thermal expansion can be manipulated using internal structures. The external properties of the materials also can be enhanced by using optimized parameters of the unit cells such as the shape of the unit cell, size and unit cell orientation, etc. Hence by changing the internal geometry of the material we can control its properties. Metamaterials research has involved broader areas such as optics, communication, biomedical, and so on. Metamaterials are generally classified as electromagnetic, mechanical, acoustic, and thermal metamaterials [2-5].

Mechanical metamaterials are man-made materials that derive their unusual properties from the geometry of building blocks rather than the properties of their constituents [6]. The derived unusual properties of these metamaterials include negative rigidity, negative poisson's ratio, negative squeezability, and fading shear modulus [7]. Mechanical metamaterials are further classified as Auxetic, Penta-Mode, and Origami-Based Metamaterials.

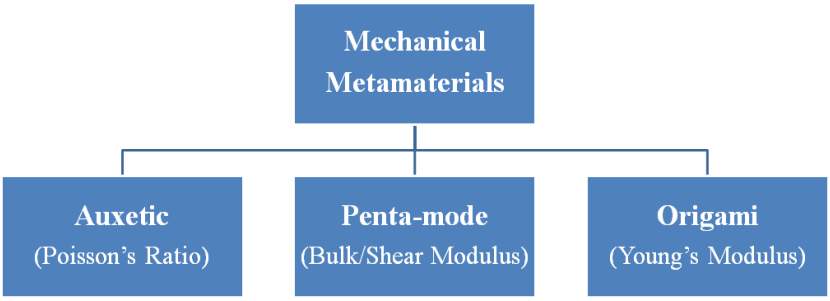

Fig. 1: Mechanical metamaterials classification

The auxetic metamaterials are associated with a negative poisson's ratio and become thicker normal to the applied force when stretched. This is possible only due to their internal structure and the way they deform under uniaxial loading. Gibson et al invented the first conventional re-entrant Metamaterial structure in 1982 [8]. Apart from re-entrant various other types of auxetic Metamaterial have been developed such as chiral, rotating polygon, etc. as explained by Liu Y et al. [9]. According to the authors Parth Uday Kelkar, et al. [10] materials have different poisson's ratio depending upon their internal geometry. Auxetic metamaterials are used in bio-medicine, soft robotics, and acoustics. As per Kolken, et al. [11] these materials also find applications in the areas of automotive, aerospace, and defense industries due to their improved shock absorbance properties. Based on the unit cells used in printing, various types of auxetic metamaterials were discussed by Xin Wu et al. [12]. Another class of mechanical metamaterials is Penta-mode Metamaterial which is classified based on bulk/shear modulus properties. Normally Penta-mode metamaterials have a larger bulk modulus in comparison with their shear modulus and have a poisson's ratio value of 0.5[13-16]. On the other hand, the Origami metamaterials which are derived from Japanese paper folding art find their applications in bio-medical stents and self-folding robotic devices [17-19].

As the auxetic mechanical metamaterials are finding more significance in recent times, there is a huge demand for the development of new metamaterial models based on their auxeticity to cater to a wider spectrum of applications. To explore and develop new mechanical metamaterials, it has been decided to conduct an experimental investigation on 3D printed mechanical metamaterials and study their mechanical properties. In the current work presented in this paper an attempt is made to experimentally investigate the two established auxetic mechanical metamaterial models namely chiral and re-entrant. Also based on these models a hybrid metamaterial model (*Anti-tetra chiral*) was developed and tested under a uniaxial compression test to study its mechanical properties and compare it with the well-established chiral and re-entrant models.

2. Experimentation

2.1 3D Printing of Mechanical Metamaterial Models

All three models chiral, re-entrant, and hybrid as shown in Figure 2 were fabricated using Stratasys F120TM 3D-printer. The parameters like bed temperature, nozzle temperature, printing speed, infill density were all held to constant values as these are the default settings in Stratasys F120^{TM} 3D-printer according to the material selected. The printed models were cured before mechanical testing by keeping them at room temperature for about 24 hours.

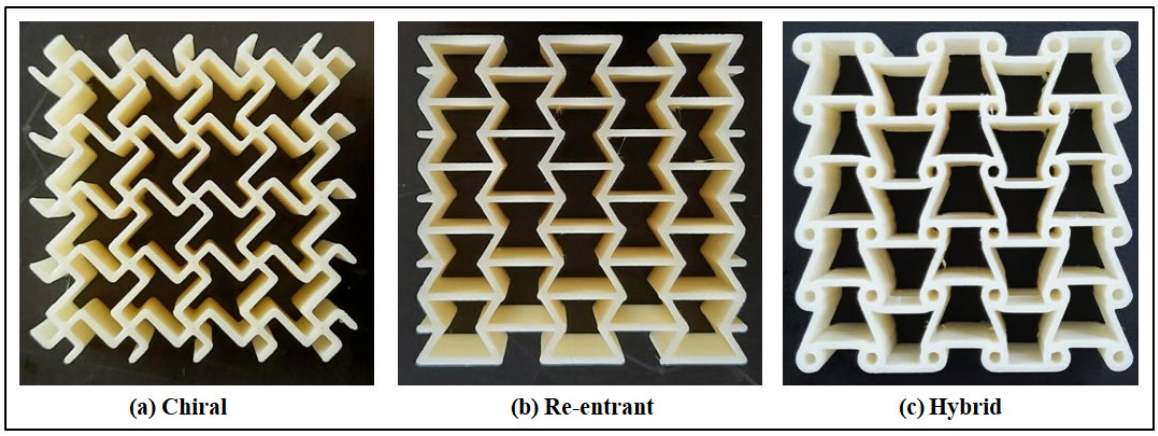

Fig. 2: 3D Printed Mechanical Metamaterials (a) Chiral, (b) Re-entrant, and (c) Hybrid Model

In this study, Acrylonitrile Styrene Acrylate (ASA) filament was used to fabricate the samples using the FDM process. ASA material is selected over ABS (acrylonitrile butadiene styrene) which is normally used in recent FDM fabrication as it displays better mechanical properties compared to ABS material. The properties of ASA material are tabulated below in Table 1.

Table 1: Properties of ASA

Properties	**Typical values**
Glass Transition Temp.	112 ^{0}C
Density	1.08 g/cm^3
Compressive Strength	75 MPa
Young's Modulus	2.5 GPa

The Chiral, Re-entrant, and Hybrid Metamaterial models (Fig. 2) were fabricated by varying printing layer height (0.178mm and 0.254mm) with a constant rib thickness of 0.75 mm. The other dimensions of the models are given in Table 2.

Table 2: Dimensions of Metamaterial models

Model	**Length, l**	**Width, w**	**Height, d**
Chiral	50.59	50.59	20.80
Re-entrant	50.76	47.13	20.00
Hybrid	49	49	20.00

2.2 Uniaxial Compression Testing of Printed Models

To investigate the mechanical behavior of all three metamaterials, a uniaxial compression test was conducted using BISS UTM with 100 kN load carrying capacity. The models were tested under two different strain rates of 0.5 % (5×10^{-3} s^{-1}) and 1 % (10×10^{-3} s^{-1}). Figure 3 shows the deformation of 3D printed metamaterials under the uniaxial compression test.

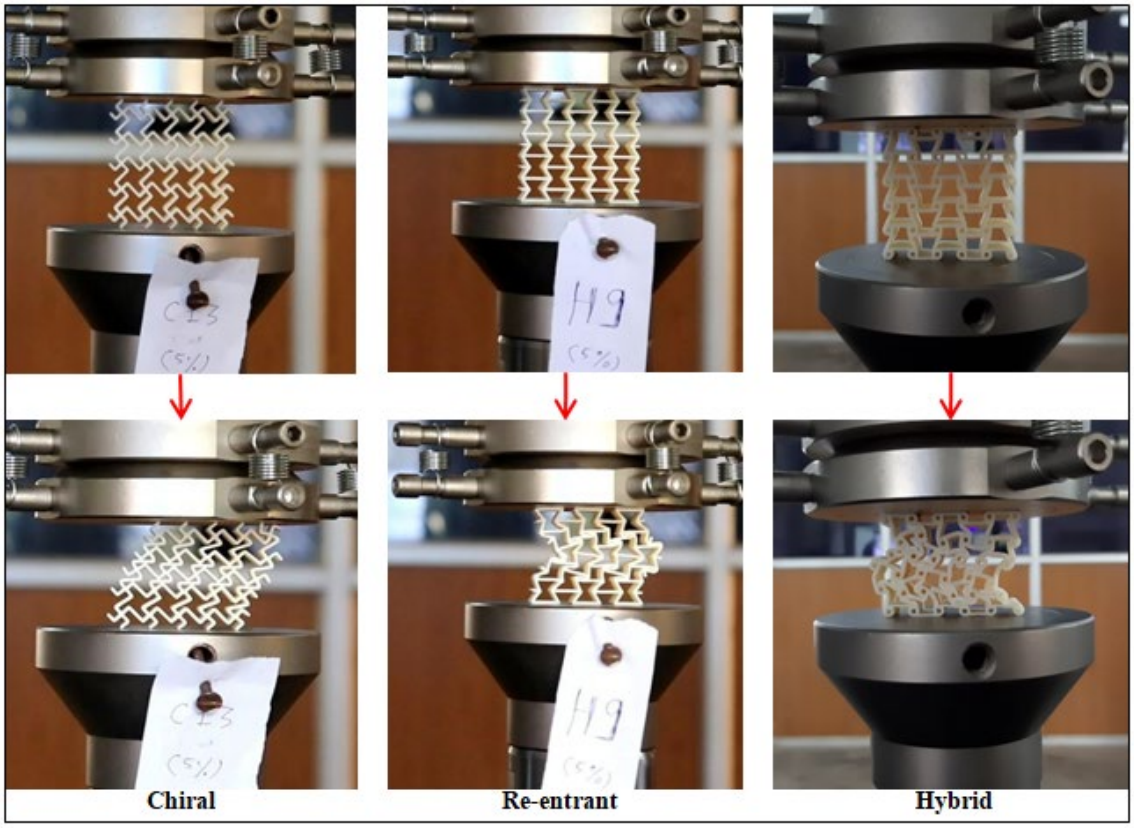

Fig. 3: Deformation of printed metamaterials under uniaxial compression test with 0.5% s^{-1} strain rate

2.3 Simulation Study:

The deformations of the designed models were studied through quasi-static analysis using ANSYS software. The deformation modes of the models is given in Figure 4.

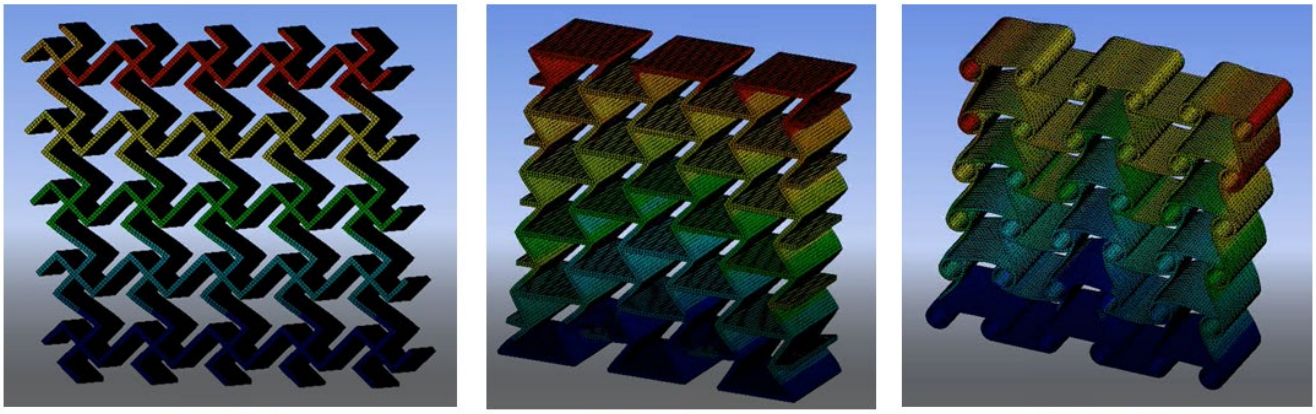

Fig. 4: Deformation modes of models

2.4 Ex-situ Characterization:

The printed models after undergoing uniaxial compression tests are characterized using scanning electron microscopy (SEM) to study the crack and fracture morphology of the models. Different fracture and crack propagations were observed and are discussed in the next section.

Abbreviations used:
C0.178_0.75mm_0.5% [R stands for Re-entrant and H stands for Hybrid Model]
Chiral with 0.178 mm layer height and 0.75mm rib thickness tested under 0.5% strain rate

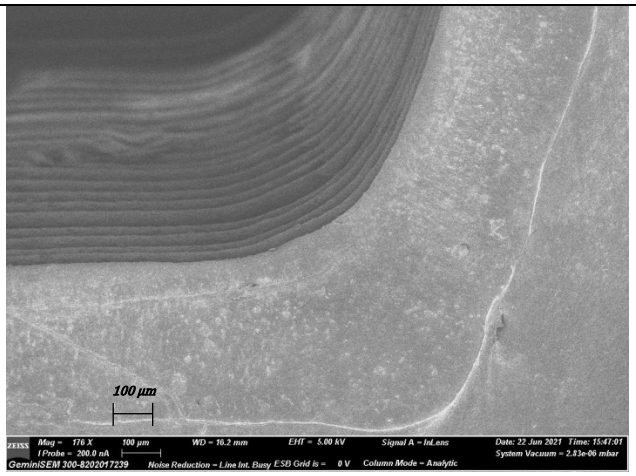

Chiral Before Test : C0.178_0.75mm_0.5%

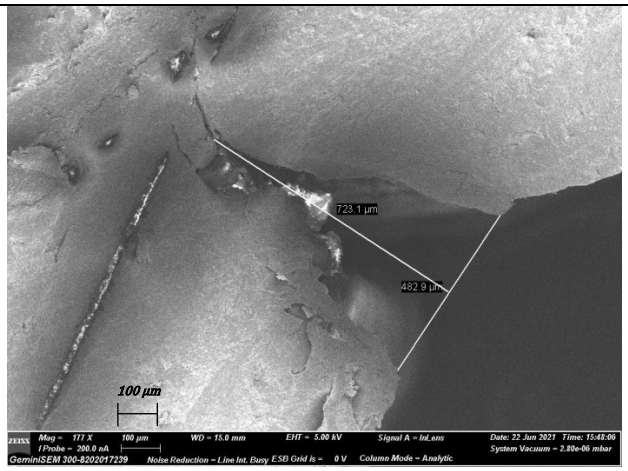

After Test : Crack depth ratio is 0.964

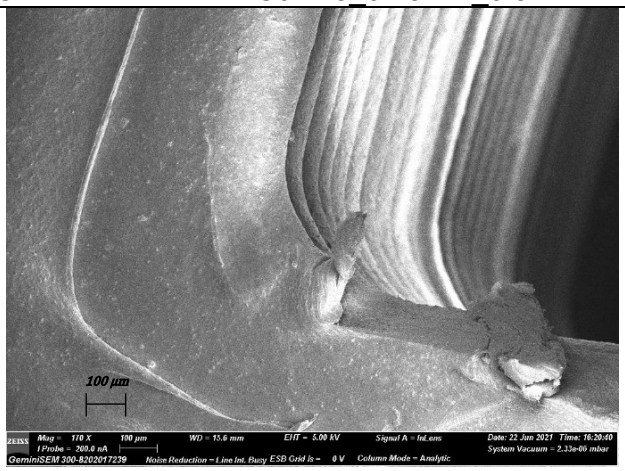

Chiral Before Test : C0.254_0.75mm_0.5%

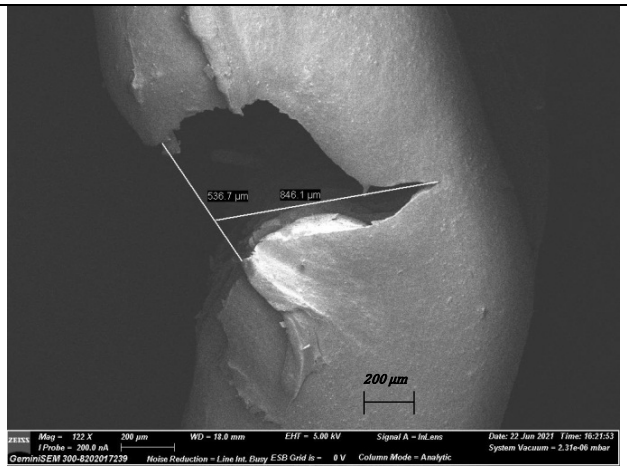

After Test : Crack depth ratio is 1.128

(a). Images of cracks developed in Chiral Models

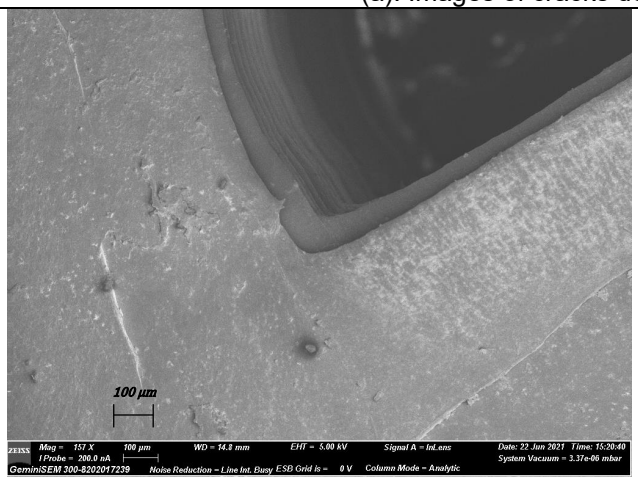

Re-entrant Before Test : R0.178_0.75mm_0.5%

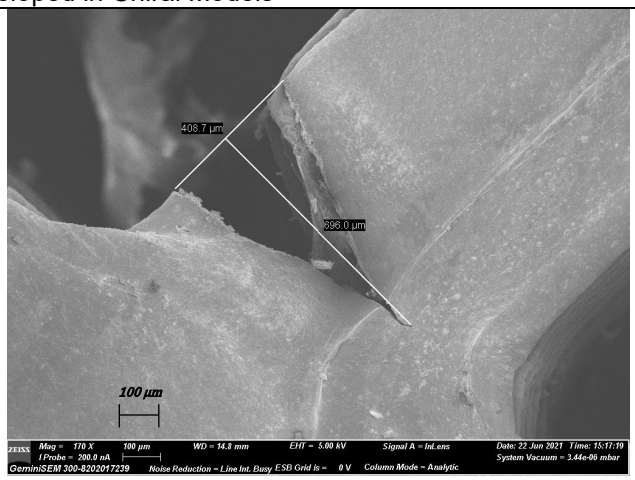

After Test : Crack depth ratio is 0.928

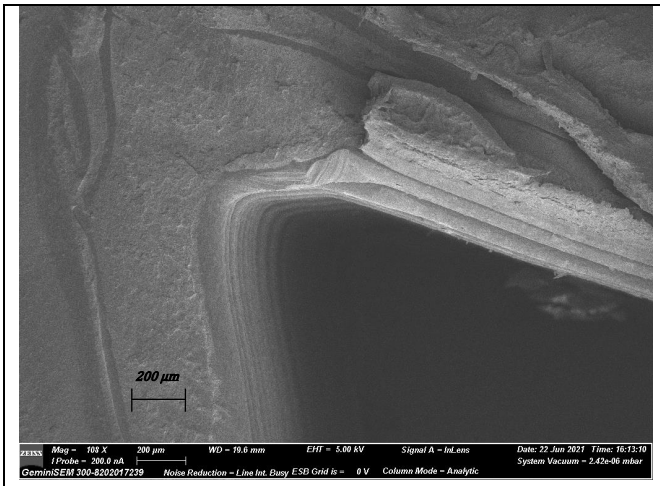

Re-entrant Before Test : R0.254_0.75mm_0.5%

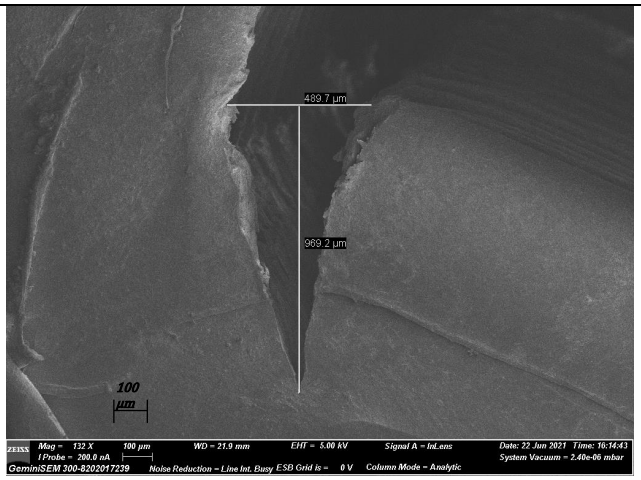

After Test : Crack depth ratio is 1.292

(b). Images of cracks developed in Re-entrant Models

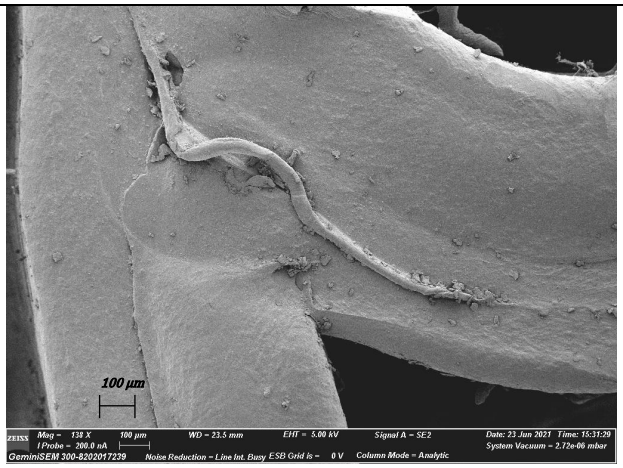

Hybrid Before Test : H0.178_0.75mm_0.5%

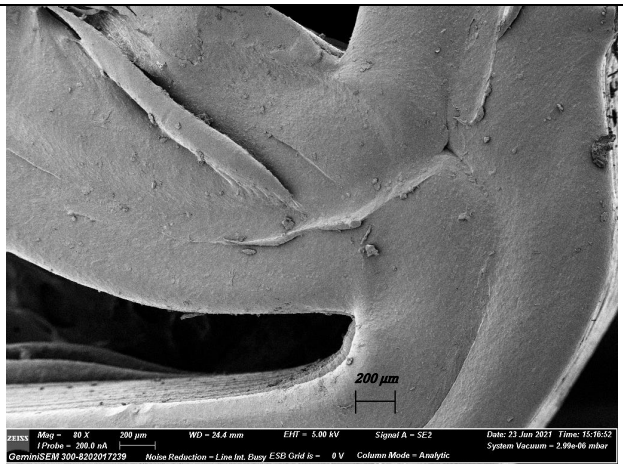

Hybrid Before Test : H0.254_0.75mm_0.5%

(c). Images Ribs in Hybrid Models

Fig. 5: Crack morphology of the models

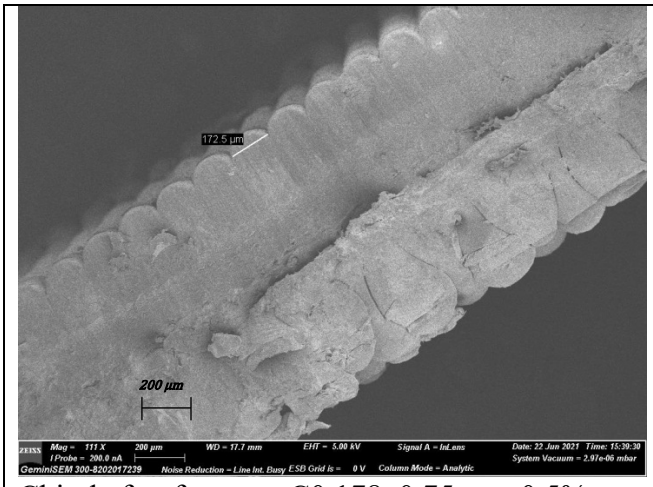

Chiral after fracture: C0.178_0.75mm_0.5%

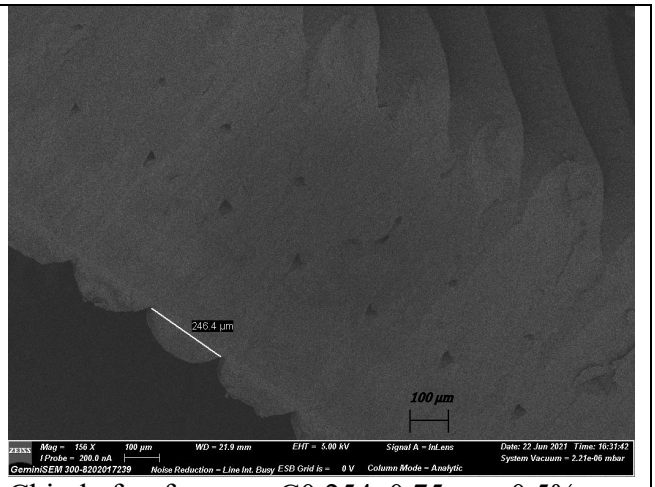

Chiral after fracture: C0.254_0.75mm_0.5%

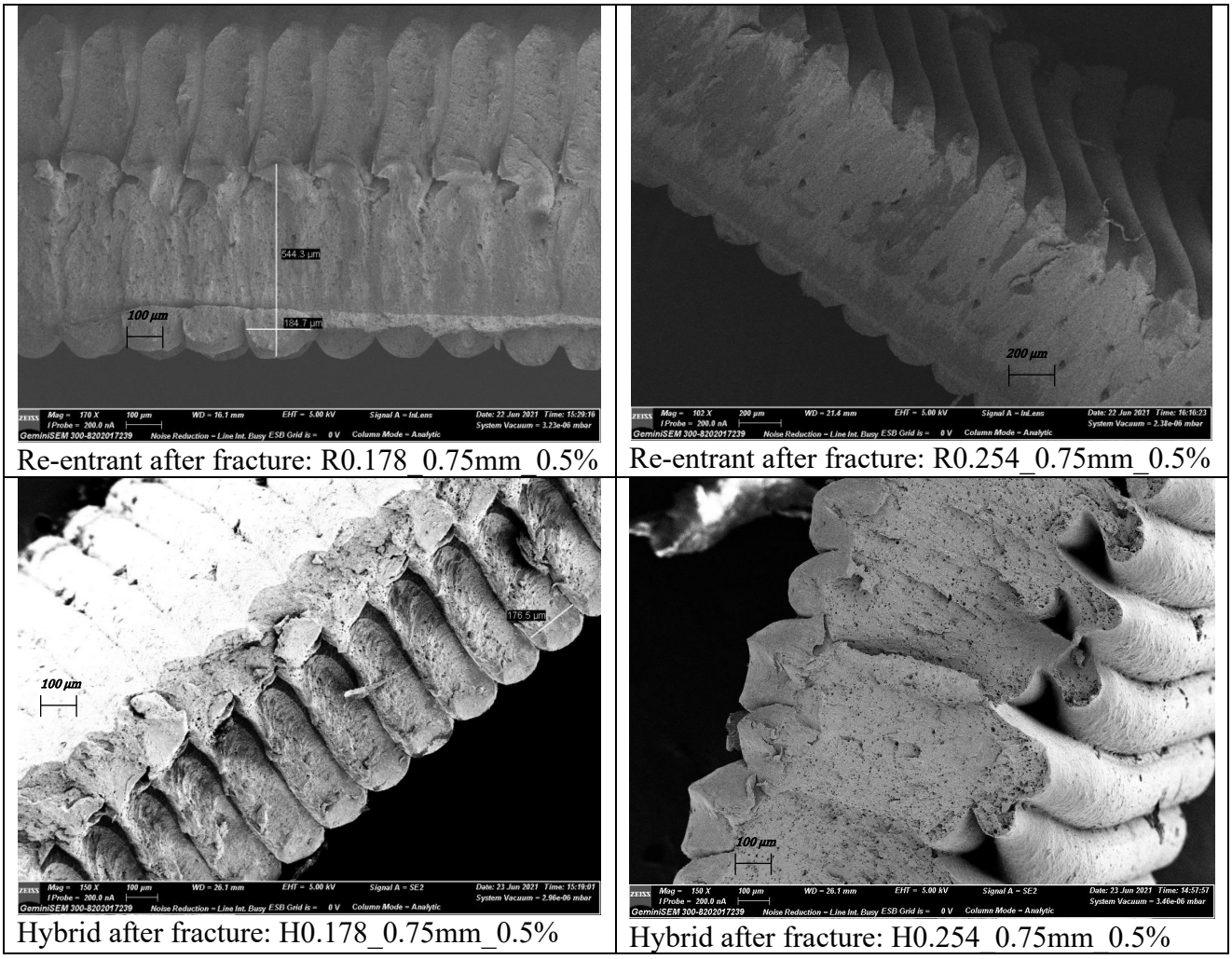

Fig. 6: Fracture morphology of the models

3. Results and Discussion

A uniaxial compression test was conducted on all three metamaterial models as shown in Figure 3 to compare the mechanical behavior of the models and to investigate the effect of layer height on their mechanical properties.

The deformation modes under uniaxial compression tests were modeled using ANSYS software as shown in Figure 4 & compared with experimental results. The images of the cracks developed after testing as shown in Figure 5 prove that, progressive crack propagation is observed in both the chiral and re-entrant models. Whereas in the case of the hybrid model the failure is due to brittle fracture. Crack depth ratio (length of crack/rib thickness) of 0.964 & 1.128 is observed in the case of the chiral model printed with a layer height of 0.178 mm & 0.254 mm respectively. Whereas re-entrant model has shown the crack depth ratio of 0.928 mm & 1.292 mm for layer height of 0.178 mm & 0.254 mm respectively.

Figure 6 shows the fracture morphology of models after the uniaxial compression test. In the chiral model, a combination of inter and intra-laminar fracture was observed for 0.178 mm layer height whereas for 0.254 mm layer height only intra-laminar fracture was observed leading to the uniform fractured surface. A similar trend is also observed in the Re-entrant model. But for the hybrid model in both layer height cases, a combination of inter and intra-laminar fracture were observed. This may be attributed to the brittle fracture that occurred during testing.

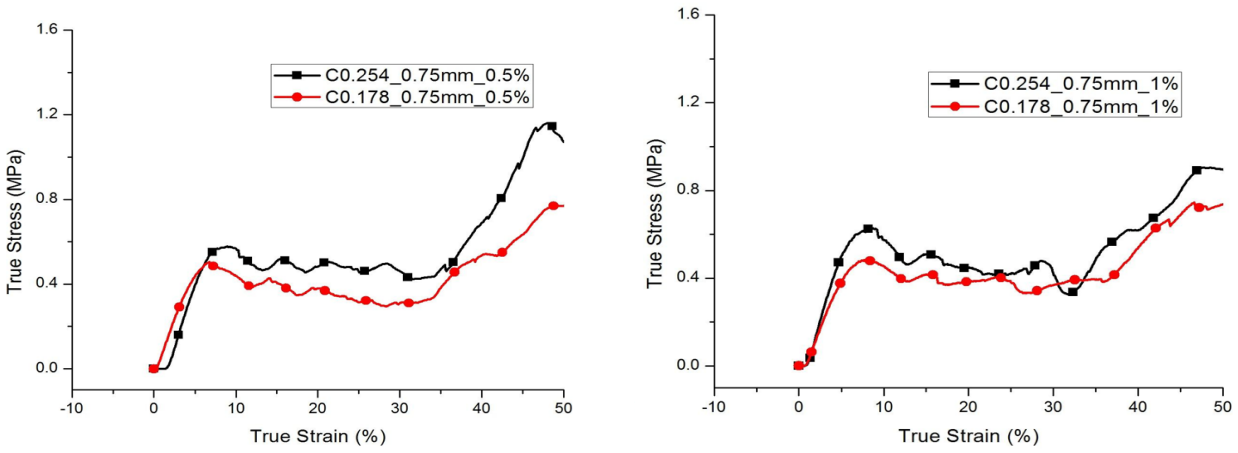

(a) Chiral

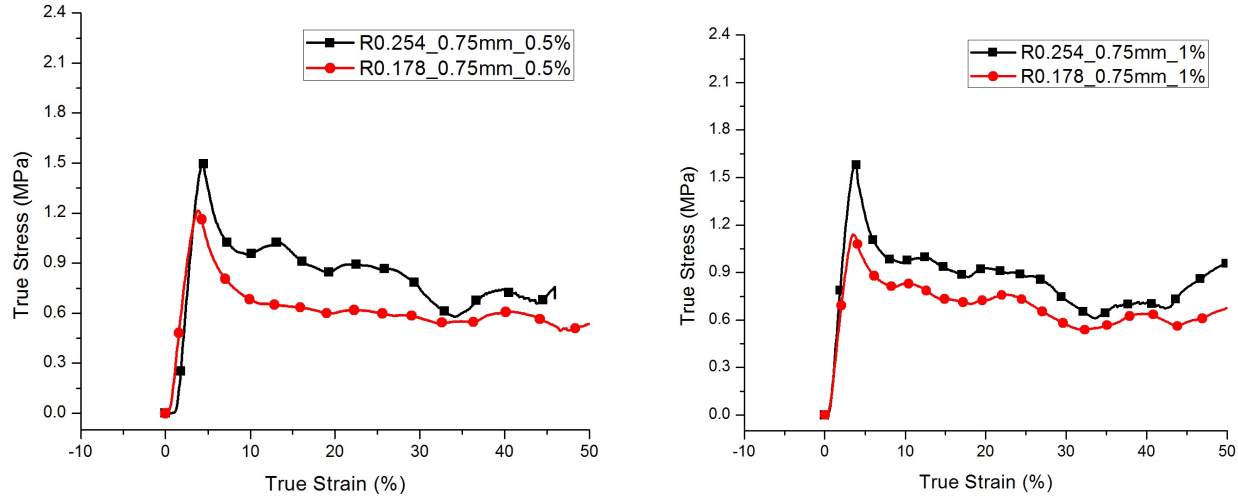

(b) Re-entrant

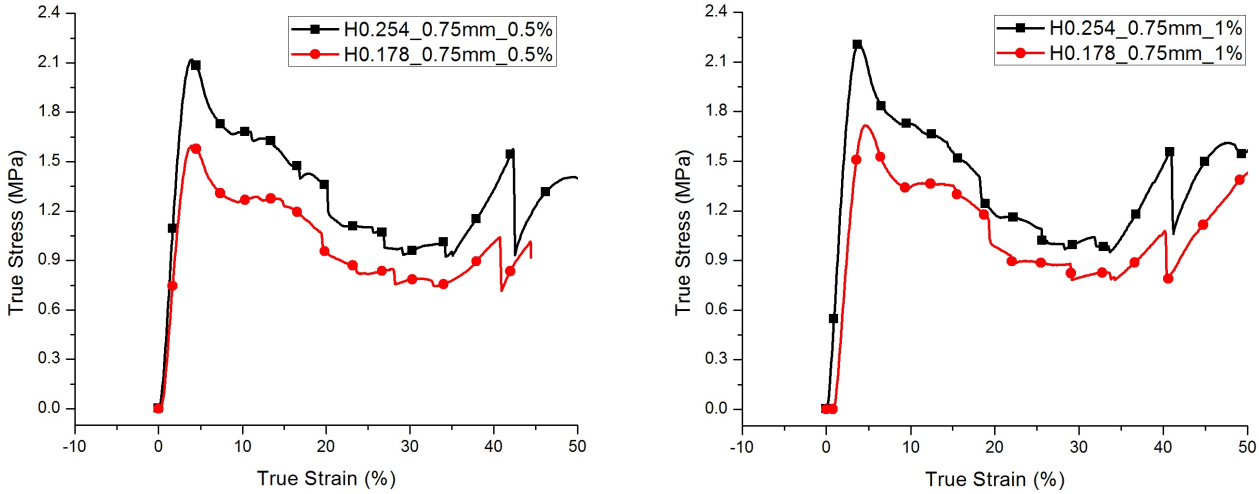

(c) Hybrid

Fig. 7. Effect of layer height used for printing on the true stress-strain relationship under strain rate of 0.5% s^{-1} and 1% s^{-1} respectively.

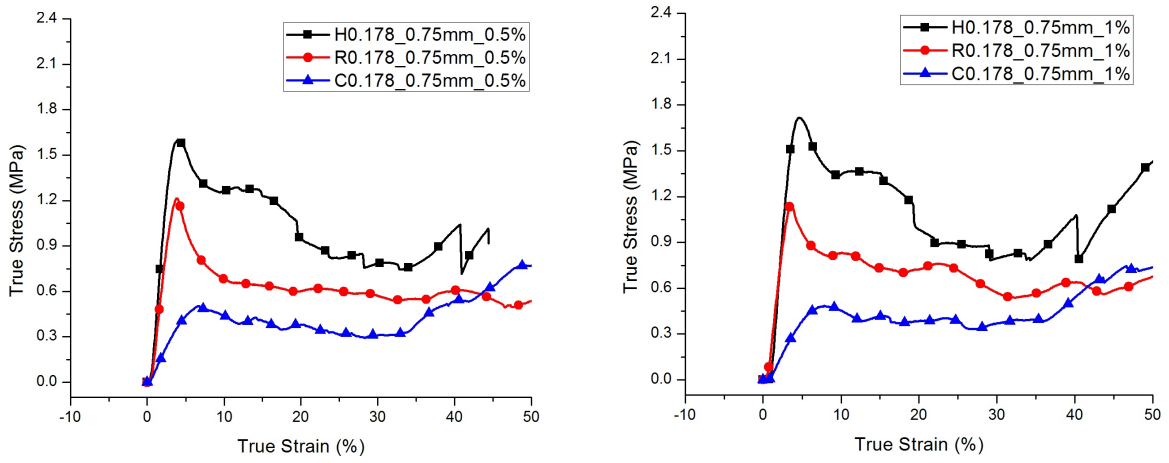

(a)

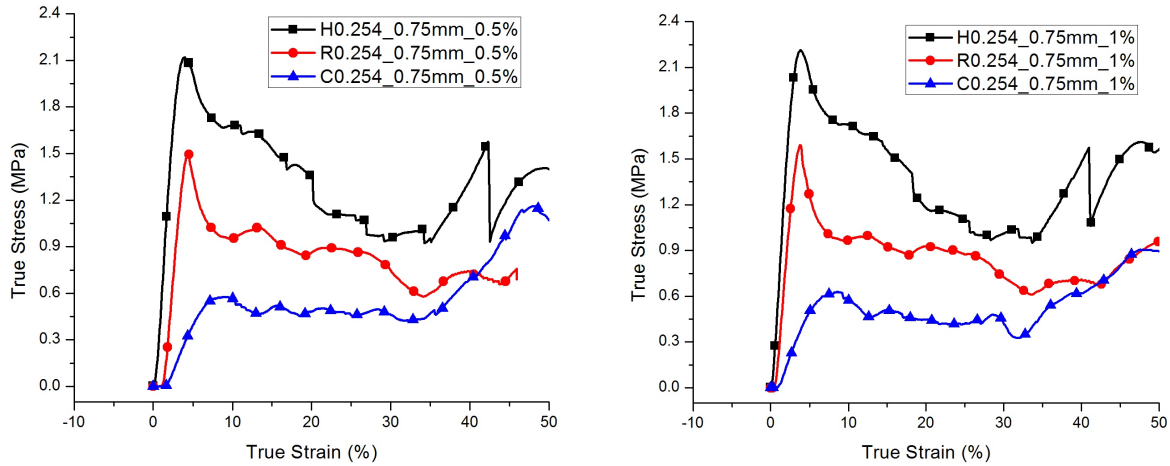

(b)

Fig. 8. True stress-strain relationship between hybrid, re-entrant, and chiral models printed using a layer height of (a) 0.178 mm
and (b) 0.254 mm under strain rate of 0.5% s^{-1} and 1% s^{-1} respectively.

The effect of layer height used in the printing of the models is studied and is shown in Figure 7. As it is evident from the above shown figures that an increase in the strain rate from 0.5 % to 1 % has no significant effect on the mechanical properties. With an increase in layer height of around 30 %, there is an increase in peak stress of 16 %, 25 %, and 40 % for chiral, re-entrant, and hybrid models respectively. This can be attributed to the reduction of interfaces between the layers.

For the chiral model fabricated with a layer height of 0.178 mm as shown in Figure 8 (a), during a uniaxial compression test, the stress increases to a peak value of 0.6 MPa at around 10 % of strain and then maintains more or less this value till 35 % strain due to the self-contact between the ribs. Hardening of the chiral structure occurs beyond 35 % strain. Whereas in re-entrant model, peak stress of 1.2 MPa was observed at 5 % strain followed by a sudden drop till 10 % strain and maintaining it with minor softening. Once the strain crosses ~45%, the hardening takes place. And for hybrid (Anti-tetra chiral) model, the stress increases linearly to a peak value of around 1.8 MPa at 10 % strain and then slowly reduces and reaches almost half the peak value at 35 % strain and hardens. The hardening of structures occurs at 35 % strain for both chiral and hybrid models, whereas for re-entrant the hardening occurs at around 45 % strain. A similar trend has been observed for the models printed with a layer height of 0.254 mm as shown in Figure 8 (b). The sudden drop in the stress value

in the case of re-entrant may be attributed to the reduction in auxetic effect due to its instability under small deformation (~4%). Whereas in the case of the chiral model, the hardening occurs earlier compared to re-entrant due to drastic reduction in its volume under test and it conserves the auxetic effects as reported by Yunyao Jiang et al. [20].

It is evident from Figure 8 that the hybrid model (Anti-tetra chiral) has shown better stiffness compared to both chiral and re-entrant models and has shown an improved chirality as compared to the re-entrant model. This can be attributed to the anti-chirality nature of the structure.

4. Conclusion

The fused deposition modeling (FDM) process was used for the fabrication of three different mechanical metamaterial models namely chiral, re-entrant, and hybrid (Anti-tetra chiral). The layer height effect on the mechanical properties of all three models were studied and observed that the increase in layer height increases the strength of the models. Also, a hybrid model which is a combination of both chiral and re-entrant models was developed successfully and tested. It is observed from the results of the experimentation that the hybrid model has shown better mechanical properties as compared to chiral and re-entrant models. This shows that the improved properties can be achieved by changing and combining the properties through its structure depending upon the required application. Also in this, for both chiral and re-entrant models a combination of inter and intra-laminar fracture was observed for 0.178 mm layer height. Whereas for 0.254 mm layer height only intra-laminar fracture was observed leading to the uniform fractured surface. And in hybrid model a combination of inter and intra-laminar fracture were observed.

5. Acknowledgements

This work is supported by the Science and Engineering Research Board, Department of Science & Technology, Government of India, under Start-up Research Grant (SRG) scheme (Project no: SRG/2019/000990). The authors also gratefully acknowledge partial funding support from Indian Institute of Technology Dharwad, Dharwad, India under SGNF scheme.

6. References

[1]. Koschny T, Soukoulis C M and Wegener M, Metamaterials in microwaves, optics, mechanics, thermodynamics, and transport J. Opt. 2017, 19 084005

[2]. Fedotov V 2017, Metamaterials Springer Handbook of Electronic and Photonic Materials (Springer Handbooks)

[3]. Katia Bertoldi, Vincenzo Vitelli, Johan Christensen, and Martin van Hecke, 2017. Flexible mechanical metamaterials. Nature Reviews Materials, 2 (17066), pp. 1-11

[4]. Wong Z J, Wang Y, O'Brien K, Rho J, Yin X, Zhang S, Fang N, Yen T J and Zhang X 2017 Optical and acoustic metamaterials: superlens, negative refractive index and invisibility cloak J. Opt. 19 084007

[5]. Sklan S R and Li B 2018 Thermal metamaterials: functions and prospects Natl Sci. Rev. 5 138–41

[6]. Xu X, Zhou J, Liang H, Jiang Z and Wu L, Mechanical metamaterials associated with stiffness, rigidity and compressibility: a brief review Prog. Mater Sci. 2018, 94 114–73

[7]. Nicolaou Z G and Motter A E, Mechanical metamaterials with negative compressibility transitions Nat. Mater. 2012, 11 608–13

[8]. Gibson L J, Ashby M F, Schajer G S and Robertson C I, The mechanics of two-dimensional cellular materials Proc. R. Soc. A, 1982, 382 25–42

[9]. Liu Y and Hu H, A review on auxetic structures and polymeric materials Sci. Res. Essays , 2010 , 5 1052–63

[10]. Parth Uday Kelkar, Hyun Soo Kim et al. Cellular Auxetic Structures for Mechanical Metamaterials: A Review, Sensors 2020, 20, 3132

[11]. Kolken H M A and Zadpoor A, Auxetic mechanical metamaterials RSC Adv. 2017, 7 5111–29

[12]. Xin Wu , Yutai Su and Jing Shi, Perspective of additive manufacturing for metamaterials development, Smart Mater. Struct. 2019, 28 093001

[13]. Zadpoor A A , Mechanical Metamaterials. Mater Horiz. 2016, 3, 371–381

[14]. M. Kadic, T. Bu¨ckmann, N. Stenger, M. Thiel and M. Wegener, On the practicability of pentamode mechanical metamaterials, Appl. Phys. Lett., 2012, 100, 191901

[15]. R. Schittny, T. Bu¨ckmann,M. Kadic andM.Wegener, Elastic measurements on macroscopic three-dimensional pentamode metamaterials, Appl. Phys. Lett., 2013, 103, 231905

[16]. A. A. Zadpoor, Bone tissue regeneration: the role of scaffold geometry, Biomater. Sci., 2015, 3, 231–245

[17]. Schenk M, Guest SD 2013 Geometry of Miura-folded Metamaterials. Proc Natl Acad Sci U S A. 2013, 110, 3276–3281

[18]. S. Felton, M. Tolley, E. Demaine, D. Rus and R. Wood, A method for building self-folding machines, Science, 2014, 345, 644–646

[19]. K. Kuribayashi, K. Tsuchiya, Z. You, D. Tomus, M. Umemoto and T. Ito, et al., Self-deployable origami stent grafts as a biomedical application of Ni-rich TiNi shape memory alloy foil, Mater. Sci. Eng., A, 2006, 419, 131–137

[20]. Y. Jiang, B. Rudra and J. Shim et al., Limiting strain for auxeticity under large compressive deformation: Chiral vs. re-entrant cellular solids, International Journal of Solids and Structures, 2019, 162, 87–95

*****